TERRAIN-RELATED WALKING DEMAND AND SUMMER ENVIRONMENTAL EXPOSURE ON HIKING ROUTES IN TWO ROMANIAN MOUNTAIN REGIONS

***Zsolt MAGYARI-SÁSKA*[1] *& Lóránt BÁLINT-BÁLINT*[1]**

DOI: 10.21163/GT_2027.221.16

ABSTRACT

Mountain hiking routes with similar terrain demands can differ considerably in their summer environmental setting. We assessed 103 archived routes in the Harghita–Gurghiu–Călimani region (HGC; 67 routes) and the Apuseni Mountains (36 routes), using GPX tracks, Copernicus elevation data, 2023 Tree Cover Density and ERA5-Land summer temperatures for 1991 – 2020. The Terrain-related Navigation Index (TNI) represented slope-related walking demand through normalized bidirectional Tobler pace, while the Potential Heat-exposure Index (PHI) combined background temperature, geometric solar potential and canopy openness. Segment scores were aggregated into length-weighted route means, with each itinerary receiving equal weight in regional comparisons. Median TNI was 0.151 in the HGC region and 0.228 in the Apuseni Mountains, giving a difference of −0.077 and a 95% spatial block-bootstrap interval of 0.107 to −0.028. Median PHI was 0.498 and 0.529, respectively; its smaller contrast of −0.031 had an interval from −0.144 to 0.047. Cooler background temperatures in the HGC region offset greater solar potential and openness under the reference weights. All 24 processing variants retained negative regional contrasts, whereas 231 component-weight combinations produced PHI contrasts ranging from −0.254 to 0.114. Three route examples showed how similar exposure scores can accompany markedly different distances and lengths of continuous open terrain. For walking tourism, the paired indices and route profiles provide a basis for descriptions that explain environmental conditions alongside terrain demand and modelled duration.

Keywords*: Outdoor recreation; Spatial dependence; Multicriteria assessment; Canopy cover; Uncertainty analysis.*

1. INTRODUCTION

Summer walking conditions can differ considerably between paths with similar distance and ascent, particularly where an itinerary moves between open pasture and sections beneath trees. These changes in cover are part of the visitor's experience, and their location along a route adds useful context to the effort described by its distance and ascent. Bringing canopy cover and the local summer environment into the route description gives managers a fuller account of the walk to share with visitors.

Walking tourism links paths with accommodation, local guiding and access to landscape and heritage (UNWTO, 2019). In 2024, Romanian accommodation establishments recorded 12.2 million domestic and 2.4 million international overnight visitors (OECD, 2026), illustrating the importance of the domestic market within the national tourism economy. Tourism policy also prioritises rural products, ecotourism and destination-level management. For walking destinations, route descriptions can support these offers by explaining terrain demand and summer environmental conditions alongside distance and ascent.

[1] *Faculty of Geography, Babeș-Bolyai University, Cluj-Napoca, Romania, zsolt.magyari@ubbcluj.ro (ZMS); lorant.balint@ubbcluj.ro (LBB)*

The relationship between effort and exposure also matters for climate adaptation, since tourism vulnerability depends on local conditions and the capacity to adapt (Scott et al., 2019). Research on heat-related illness among Grand Canyon visitors linked observed health outcomes to daily weather and visitation records (Buttke et al., 2023). Our study approaches the summer walking environment through archived geographical layers, comparing the relative conditions along selected Romanian mountain routes.

GIS-based multicriteria methods offer an established approach to comparing recreational environments (Malczewski, 2006; Fung & Wong, 2007). At the Racoș Geological Complex, Lakatos and colleagues used activity-specific spatial criteria to identify suitable locations for ecotourism facilities and thematic hikes (Lakatos et al., 2023). Using individual hiking itineraries as the unit of comparison, this study provides a reproducible assessment of terrain demand and summer environmental exposure in the Harghita–Gurghiu–Călimani (HGC) region and the Apuseni Mountains, treating these as separate dimensions and distinguishing the sensitivity of regional contrasts to processing choices from their sensitivity to PHI component weights.

2. STUDY AREAS AND DATA

The eastern catalogue comprises selected routes associated with the Harghita, Gurghiu and Călimani mountain ranges (HGC), while the western catalogue lies in the Apuseni Mountains (**Fig. 1**). Their geographical settings offer different contexts for walking tourism: the eastern volcanic terrain has varied landforms and geoheritage (Szakács & Kovacs, 2022), and caves, karst scenery and forests are important features of the western region's visitor experience (Telbisz et al., 2023).



Fig. 1. Location of the two route catalogues within Romania. Coloured rectangles show the processing footprints of the selected catalogues.

Eastern tracks and route names were obtained from HRTracks (HRTracks, n.d.), with western tracks supplied by Salvamont Bihor and Bihor în imagini (Salvamont Bihor, n.d.; Bihor în imagini, n.d.). Each archived file represents a route alternative, so different itineraries may share stretches of trail. Of the 115 retained geometries, five fragments shorter than 500 m, six geographical transition cases associated with the Vârghiș area and one long-distance itinerary were assigned to sensitivity analyses. The location of the gorge in the Perșani Mountains provides the geographical basis for

treating these cases separately, and their complete tracks were retained for the sensitivity checks (Visit Harghita, n.d.). The resulting primary sample contains 67 eastern and 36 western routes (**Fig. 2**), with all separately classified geometries included in the sensitivity analyses.

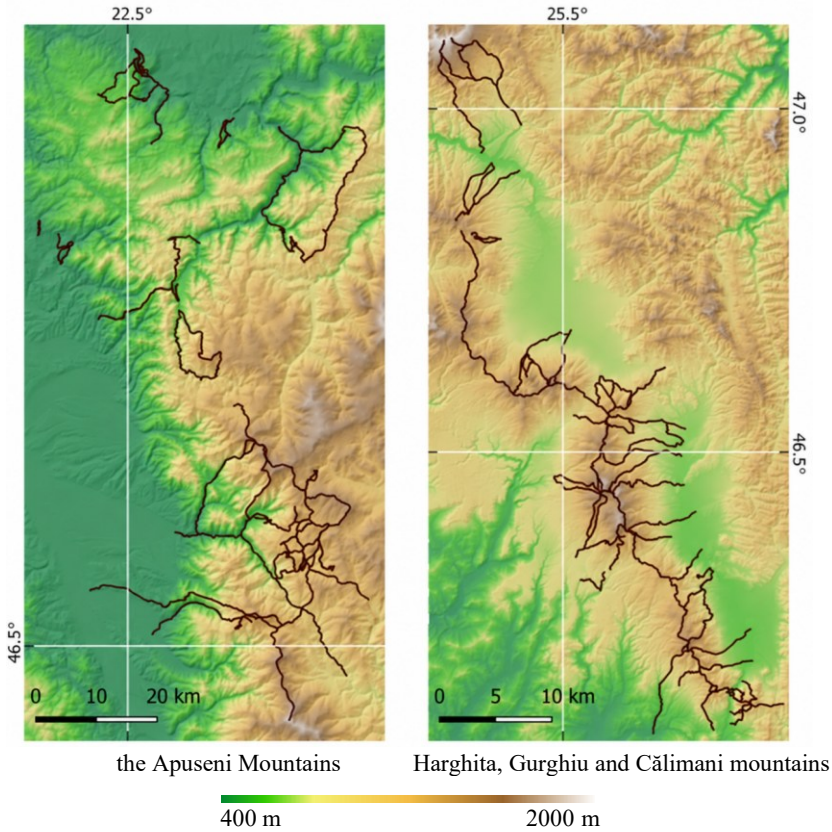


Fig. 2. Hiking routes in the Apuseni Mountains and in the HGC region.

Each environmental layer contributes a different spatial or temporal aspect of the walking environment. Copernicus DEM GLO-30 provides a digital surface model at approximately 30 m, including vegetation and structures in its elevation values (Copernicus Data Space Ecosystem, n.d.), and the archived approximately 10 m Tree Cover Density (TCD) service extracts describe projected crown cover for 2023 (CLMS, 2024). For the climatic background, monthly ERA5-Land 2 m air temperatures on a 0.1° grid were used to calculate month-length-weighted summer means for 1991–2020 (Muñoz-Sabater et al., 2021; C3S, 2019).

3. METHODS

The analysis follows a two-index framework that brings together the terrain and environmental characteristics of hiking routes. The Terrain-related Navigation Index (TNI) describes slope-related walking demand, while the Potential Heat-exposure Index (PHI) combines background temperature, potential solar radiation and canopy openness. Both indices are calculated for individual route segments and then aggregated into route-level summaries, providing the basis for comparison between the HGC region and the Apuseni Mountains. The workflow describing the analysis steps in **figure 3** follows the tracks and environmental layers through to the route summaries, keeping the terrain and environmental calculations in separate branches until the catalogue comparison. At that stage, spatial resampling describes variation within the retained sample, and sensitivity checks examine how the results respond to processing and assessment choices.

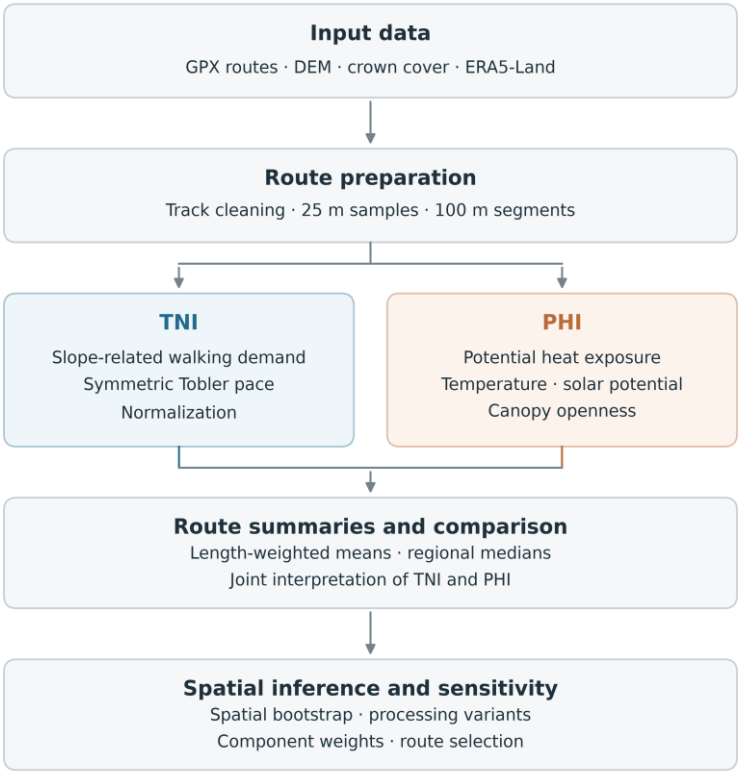


Fig. 3. Analytical workflow

3.1. Route geometry and the Terrain-related Navigation Index (TNI)

Planar distance measurements and spatial grouping used WGS 84 / UTM zone 35N (EPSG:32635) for HGC routes and zone 34N (EPSG:32634) for Apuseni routes. Track edges were intersected with the processing footprints before distances were measured. We retained separate track runs, removed consecutive duplicate coordinates and treated edges longer than 5 km as gaps. Each retained polyline was then sampled at 25 m and divided into 100 m analysis segments, including its final partial segment. Using the polyline arc length in the slope denominator preserves the distance travelled along winding sections of the path.

Bilinear sampling of the surface model supplied the segment endpoint elevations, from which grade (g) was calculated as elevation change divided by horizontal arc length. We converted Tobler's speed function (Tobler, 1993) into forward (p_+) and reverse (p_-) pace in minutes per kilometre, then took their mean (p_{sym})

$$p_{\pm} = 10\, e^{3.5|\pm g + 0.05|}, \quad p_{sym} = \frac{p_+ + p_-}{2} \qquad [1]$$

Normalizing this symmetric pace gives the terrain index (TNI), whose value is unchanged when the route is reversed. The retained forward and reverse walking times combine gradient-dependent pace with route length, allowing the intended direction of travel to be represented alongside the symmetric comparison. Walking-speed and personal calibration studies describe variation associated with walkers and path conditions (Irmischer & Clarke, 2018; Higgins, 2021); the estimates used here refer to continuous movement under the gradient-based Tobler model. TNI consequently expresses slope-related demand per unit distance through a single component derived from grade, of which slope, ascent rate and Tobler pace are deterministic transformations.

For each route, symmetric modelled walking time was obtained by summing the products of segment length (km) and symmetric Tobler pace (min km^{-1}), then converting the total from minutes to hours. This corresponds to the arithmetic mean of the forward and reverse modelled route times.

3.2. Environmental exposure and the Potential Heat-exposure Index (PHI)

Potential summer environmental exposure was assessed through PHI, which combines background air temperature, geometric solar potential and canopy openness. These components describe complementary aspects of the walking environment: temperature establishes the regional climatic background, solar potential captures variation associated with terrain orientation and solar visibility, and openness represents the extent of projected crown cover along the route. Each component was assigned to the analysis segments before normalization and aggregation.

The temperature component was derived from archived ERA5-Land monthly mean 2 m air temperatures. Summer conditions were represented by month-length-weighted means for June–August over 1991–2020, retaining this climatological reference period throughout the comparison (Muñoz-Sabater et al., 2021; C3S, 2019).

Solar potential was calculated for the local modelled surface and integrated over the 92 days of June-August at 30-minute intervals. The calculation accounted for solar declination and Earth–Sun distance, using a solar constant of 1,361 W m^{-2}. Elevation samples taken 30 m east, west, north and south of each segment midpoint supplied the local surface orientation, while surrounding terrain was represented by a horizon sampled along 32 azimuths at six distances between 100 and 3,200 m. At each time step, direct solar contributions entered the sum when the sun was above both the astronomical horizon and the interpolated terrain horizon. Dividing the seasonal total by the number of days gave mean daily geometric solar energy in Wh m^{-2} d^{-1}. This calculation follows the geometric treatment of surface orientation and terrain visibility used in topographic radiation modelling (Dubayah & Rich, 1995; Fu & Rich, 2002). Atmospheric transmission was set to unity, giving the solar component the interpretation of direct extraterrestrial energy available to the modelled surface. Its spatial detail follows the elevation sampling and horizon discretization, whose influence was examined through the sensitivity analyses described in Section 3.3 (Ďuračiová & Pružinec, 2022).

Canopy openness (O) was calculated from the Tree Cover Density (TCD) layer as

$$O = 1 - \frac{TCD}{100} \quad [2]$$

where TCD expresses projected crown cover as a percentage. Openness therefore increases from zero under complete projected crown cover to one on fully open segments. Forest thermal-buffering studies provide the ecological basis for including canopy cover in the description of summer walking environments (De Frenne et al., 2019; Zellweger et al., 2020), with the shade experienced along a path also shaped by crown arrangement and the changing position of the sun.

Temperature and solar potential were normalized against their pooled 5th and 95th percentiles, with values outside this interval assigned to zero or one. The same normalization procedure was applied to the symmetric walking pace used for TNI in Section 3.1. To balance the two study regions and their routes, each region contributed half of the reference mass, each route received an equal share within its region, and that share was distributed among its segments in proportion to segment length. For segment (j) of route (i) in region (r), the reference mass was

$$m_{rij} = \frac{l_{rij}}{2n_r L_{ri}} \quad [3]$$

where n_r is the number of primary routes in the region, l_{rij} is segment length and L_{ri} is retained route length. This calibration gives the HGC region and the Apuseni Mountains equal influence while keeping the named itinerary as the unit of comparison.

The reference PHI was then calculated for each segment as

$$PHI = 0.35T^{*} + 0.35R^{*} + 0.30O \quad [4]$$

where T^{*} and R^{*} denote normalized temperature and geometric solar potential. The weights give temperature and solar potential equal emphasis, with canopy openness receiving a slightly smaller share. They define an approximately balanced assessment scenario whose interpretation follows both the assigned coefficients and the distributions of the three inputs (OECD et al., 2008; Greco et al., 2019).

Route-level PHI and TNI were obtained as length-weighted means of their segment scores. The additive structure of PHI allows cooler background conditions to compensate for greater solar potential or openness, so the component values were retained alongside the aggregate score in each route record.

Continuous open sections were defined as consecutive analysis segments with mean projected crown cover below 10% within the same uninterrupted track run. A segment with crown cover of 10% or more, or a gap between track runs, marked the end of a section. The length and symmetric modelled walking time of each open section were calculated by summing the lengths and modelled times of its constituent segments.

Three illustrative itineraries were selected purposively from the primary sample after examining their route-level scores and crown-cover profiles. Selection focused on contrasting combinations of terrain demand, PHI, route length and continuity of open sections. D72 combines low terrain demand with an extended open section, while D70 provides a much shorter, fully open itinerary with a similar PHI. Boga–Piatra Ciungilor–DJ 763 offers a contrasting example of higher terrain demand, lower PHI and substantial crown cover. Together, these examples support interpretation of the paired indices alongside the distance and duration of individual walks.

3.3. Spatial inference and sensitivity analysis

Regional differences were calculated as the HGC median minus the Apuseni median of route-mean scores, giving each named itinerary equal weight. Spatial resampling accounted for dependence associated with neighbouring routes, shared trail sections and common environmental grid cells. We generated 5,000 bootstrap replicates by sampling 10 km blocks defined from route centroids with replacement, separately within each region and retaining together all routes belonging to a sampled block. The resulting 95% percentile intervals describe sampling variation within the observed route datasets, with environmental inputs and model settings held fixed (Lahiri, 2003). The reference grid contained 23 occupied blocks in the HGC region and 11 in the Apuseni Mountains. Regional contrasts were calculated before rounding the route summaries.

Sensitivity to spatial grouping was examined using 20 km blocks, a half-cell shift of the 10 km grid, groups based on substantial route overlap and an independent-route resampling diagnostic (Dormann et al., 2007; Roberts et al., 2017). The overlap assessment used samples spaced at 25 m, identifying shared alignments where samples lay within 25 m of another route and local tangents differed by at most 30°, allowing opposite travel directions. A strong-overlap link required at least 500 m of matched length and coverage of at least half the length of one of the two routes.

We also fitted an ordinary least-squares model relating route-mean PHI to centred TNI and region. Further specifications included log route length, a TNI-by-region interaction and restriction to routes within the common TNI range. Spatial bootstrap intervals were calculated for the region coefficients, while residual Moran statistics were calculated separately within each region using row-standardized five-nearest-neighbour weights. Exploratory one-sided tests for positive spatial association used 4,999 permutations (Moran, 1950).

The sensitivity analysis examined how choices in the construction of the composite indicator affected regional comparisons and route rankings, following the assessment principles discussed by Saisana et al. (2005). Weight sensitivity was assessed using the reference PHI coefficients, equal component weights and a grid covering the simplex of non-negative weights summing to one.

Increments of 0.05 yielded 231 combinations, with the normalized component values held fixed throughout. Route-rank acceptability was examined through two sets of 5,000 Dirichlet samples, using Dirichlet parameters (1, 1, 1) for uniform sampling over the weight simplex and (28, 28, 24) for sampling concentrated near the reference weights (Lahdelma et al., 1998).

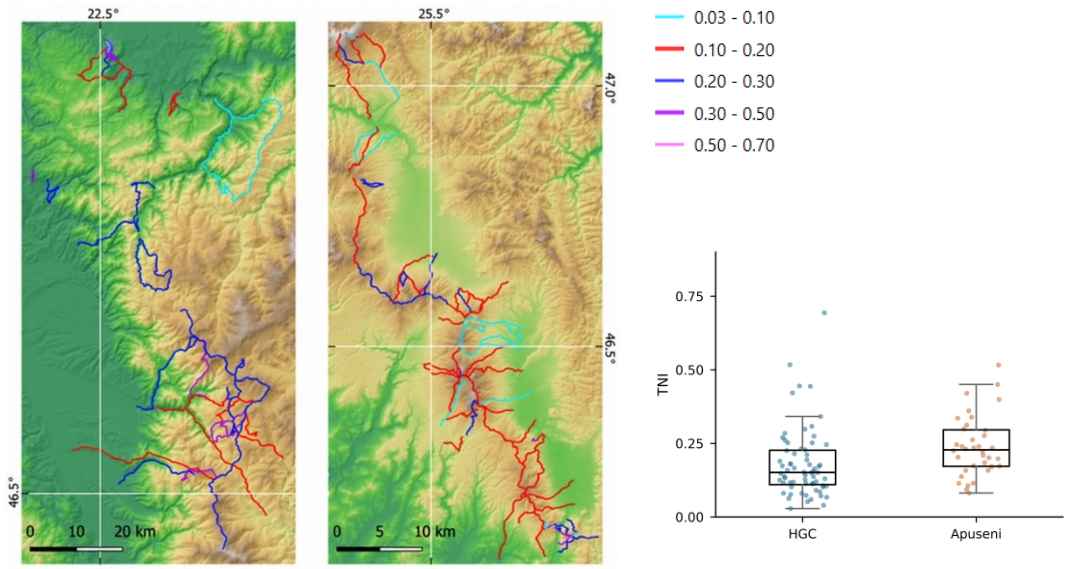
Processing sensitivity was evaluated through 24 combinations of segment spacing, elevation smoothing, normalization and horizon treatment applied to the same archived data (Steegen et al., 2016). The 50 and 200 m segment variants reused interpolated radiation estimates from the 100 m solar sampling. Separate checks compared horizons sampled along 16 and 32 azimuths, and route-selection sensitivity was assessed by extending the primary sample with geographical transition cases and short fragments.

4. RESULTS

The two regions had 103 routes divided into 11,354 segments, with 1,130.5 km of geometry comprising 712.0 km in the HGC region and 418.5 km in the Apuseni Mountains. These totals include shared stretches once for each route alternative to which they belong, and every primary segment had the inputs required for TNI and PHI. Proximity overlap was more common in the Apuseni Mountains, where the median share was 24.2%, compared with 4.6% in the HGC region. Seven routes from the HGC region and eight routes from the Apuseni Mountains had more than half their sampled length near another route, placing the grouped resampling in the context of the actual relationships among the named itineraries.

4.1. Terrain-related walking demand

Median route-mean TNI was 0.151 for the 67 HGC routes and 0.228 for the 36 Apuseni routes, giving a regional difference of −0.077 (**Fig. 4**). The lower terrain demand in the HGC region was also reflected in the median of route-mean absolute slopes, which was 4.47° compared with 5.41° in the Apuseni Mountains. Both measures therefore placed the HGC routes below the Apuseni routes in terms of slope-related walking demand. Median symmetric modelled walking time was 2.11 h in the HGC region and 2.25 h in the Apuseni Mountains.



the Apuseni Mountains | the HGC region | Points are length-weighted route means; boxes show medians and interquartile ranges.

Fig. 4. Length-weighted route-mean TNI values in the Apuseni Mountains and the HGC region.

4.2. Environmental components and PHI

The environmental components followed opposing regional patterns, with HGC routes combining lower median summer background temperature, 16.01 compared with 17.16°C in the Apuseni Mountains, and higher geometric solar potential, 10.48 compared with 10.11 kWh m^{-2} d^{-1}. These solar values express the modelled extraterrestrial geometric energy on the local surface. Median crown cover was lower in the HGC region at 49.3%, compared with 53.6% in the Apuseni Mountains. Spatial block intervals spanned zero for the temperature and crown-cover contrasts and remained positive for the geometric solar contrast. **Figure 5** retains the components in their original units, showing both their differing spreads and the lower background temperature across much of the HGC region. Higher route medians for solar potential and canopy openness accompany that cooler background, so the PHI comparison depends on how these component distributions combine under the specified weights.

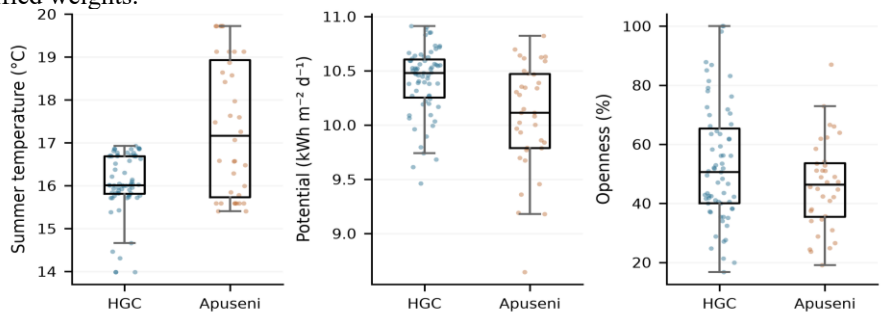
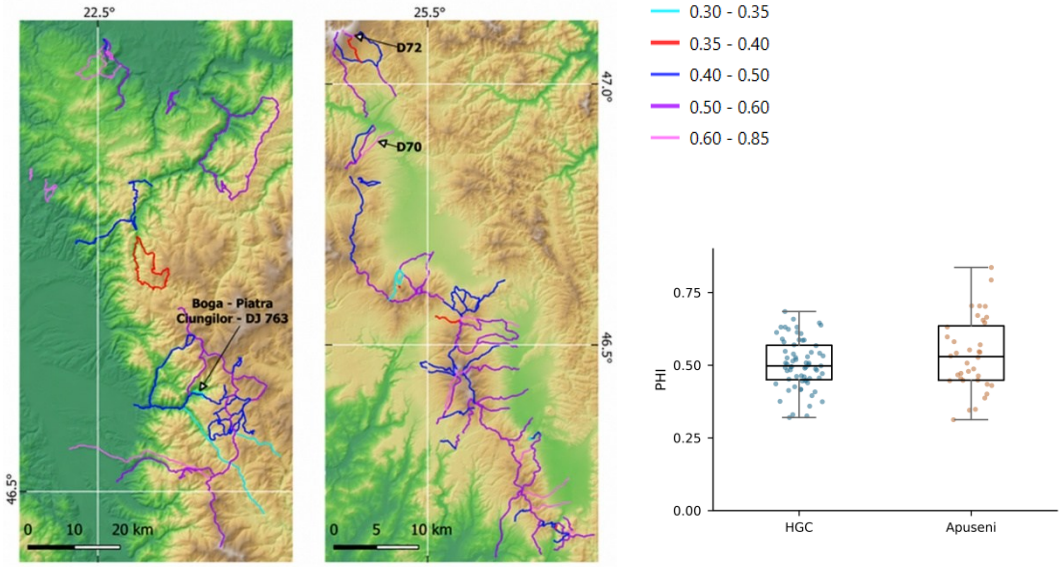


Fig. 5. Route-level environmental components in their original units. Points are length-weighted primary-route means; boxes show medians and interquartile ranges.

Under the reference weighting, median PHI was 0.498 in the HGC region and 0.529 in the Apuseni Mountains, giving a contrast of −0.031 with a 95% block interval from −0.144 to 0.047 (**Fig. 6**). This interval spans contrasts in either direction and describes the variation arising from spatial resampling of the observed catalogues under fixed environmental inputs and weights.



the Apuseni Mountains | the HGC region | Points are length-weighted route means; boxes show medians and interquartile ranges.

Fig. 6. Length-weighted route-mean PHI values in the Apuseni Mountains and the HGC region.

4.3. Joint interpretation and route examples

The joint distribution of route-mean TNI and PHI shows considerable variation in exposure among itineraries with similar terrain demand (**Fig. 7** - left). Routes near the lower end of the TNI distribution span a broad range of PHI values, reflecting differences in climatic background, solar potential and crown cover. In the model relating PHI to centred TNI and region, the HGC coefficient was −0.041, and the model explained approximately 5% of route-level PHI variation. The paired scores therefore distinguish environmental conditions among routes that occupy similar positions in terms of slope-related walking demand.

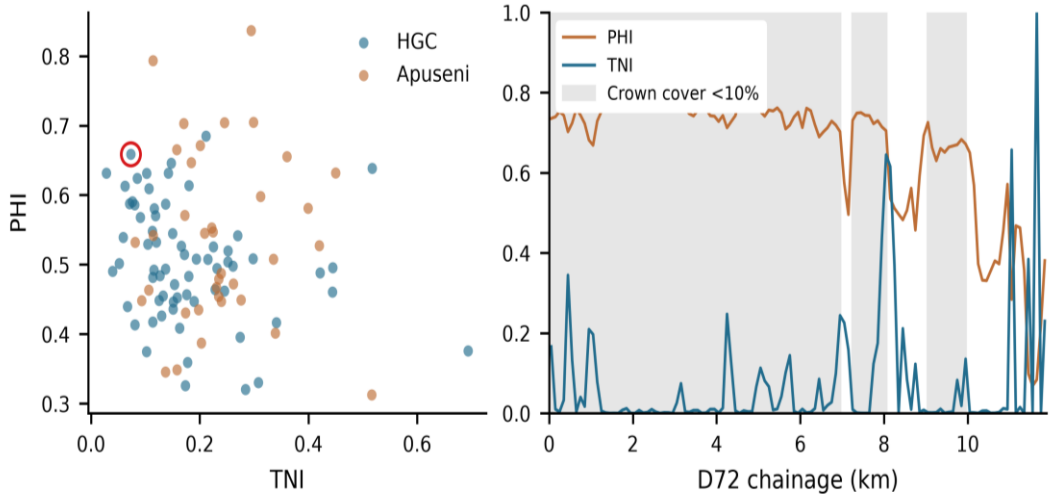


Fig. 7. Route-mean TNI and PHI (left), with D72 circled in red, and segment-level index profiles along D72 (right). Grey shading indicates projected crown cover below 10%.

The regional PHI balance can be traced through the component contributions shown in **Fig. 8**. For the difference in regional arithmetic means, normalized temperature contributed −0.093 PHI units, geometric solar potential +0.039 and canopy openness +0.021, producing a total difference of −0.033. This decomposition concerns arithmetic means, whereas the regional comparisons reported above use medians. The negative temperature contribution accounts for the lower mean PHI in the HGC region under the reference weights, with greater solar potential and openness partly offsetting that contribution.

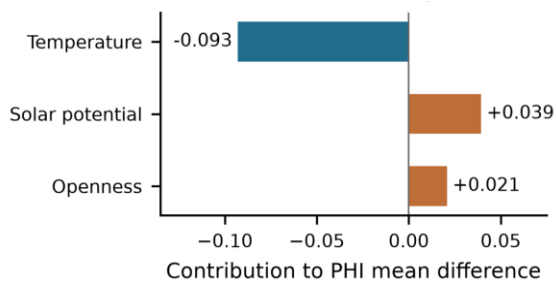


Fig. 8. Component contributions to the difference in regional mean PHI, calculated as HGC minus Apuseni.

Route D72 (highlighted by a red circle in **Fig. 7** - left), connecting Gălăuțași with Măgheruș, illustrates how these characteristics occur together along an individual itinerary. Its route-mean TNI

was 0.073 and its PHI was 0.659. Approximately 75% of the sampled length had projected crown cover below 10%, and the longest continuous section meeting this criterion extended for 7.0 km, corresponding to 1.46 hours of symmetric modelled walking time. The longitudinal profile in **Fig. 7** (right) locates these open sections within the 11.88 km route and shows how the segment-level indices vary along them. Low overall terrain demand thus accompanies an extended stretch of relatively open walking conditions.

The three routes in **Fig. 9** place the index values alongside distance, duration and crown cover. Boga–Piatra Ciungilor–DJ 763 had a TNI of 0.517 and a PHI of 0.312 over 3.28 km, with mean crown cover of 75.5% and a symmetric modelled duration of 1.21 hours. D70, from the Bradul Ciont clearing towards La Troița, had a TNI of 0.028 and a PHI of 0.631. Its retained length was 0.53 km, projected crown cover was zero throughout the sampled route, and its modelled duration was approximately 6.5 minutes. Although D70 and D72 had broadly similar route-mean PHI values, their distances and the duration of their open sections differed substantially.

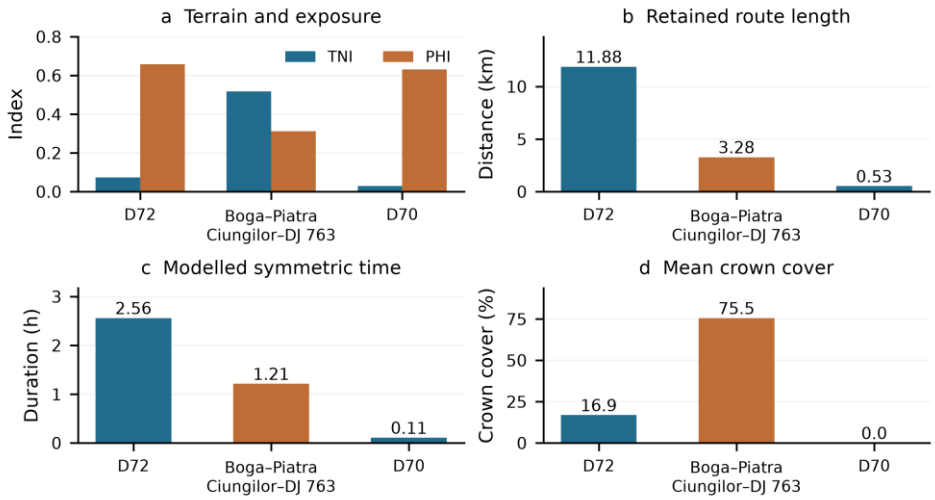


Fig. 9. Terrain and environmental characteristics of three illustrative routes: (a) route-mean TNI and PHI, (b) retained route length, (c) symmetric modelled walking time and (d) length-weighted mean crown cover.

Direction-dependent walking times supplied a further distinction among the itineraries. The median ratio of the longer to the shorter modelled directional time was 1.21 in the HGC region and 1.03 in the Apuseni Mountains. These values complement the direction-invariant TNI by describing the asymmetry of the modelled walk. At an illustrative route-mean PHI threshold of two-thirds, one HGC route and six Apuseni routes exceeded the cut-off, identifying the upper part of the exposure distribution under the reference assessment scenario.

4.4. Spatial inference and sensitivity analysis

Under the reference 10 km block resampling, the TNI contrast of −0.077 had a 95% percentile interval from -0.107 to -0.028. The intervals also remained entirely negative with 20 km blocks, a half-cell shift of the 10 km grid and groups defined by substantial route overlap. Across these spatial grouping choices, the observed terrain comparison consistently placed the HGC routes below the Apuseni routes. For symmetric modelled walking time, the median contrast was −0.134 h, with a 95% spatial block-bootstrap interval from −1.427 to 0.730 h.

The PHI intervals extended across zero under each grouping. With 20 km blocks, the interval ranged from −0.147 to 0.043; shifting the 10 km grid produced an interval from −0.158 to 0.054. Overlap-based grouping yielded a narrower interval of −0.084 to 0.041. The interval width therefore responded to the spatial grouping, while each specification retained a range encompassing regional

contrasts in both directions. Resampling individual routes independently produced a 95% percentile interval of −0.110 to −0.031 for the TNI contrast and −0.074 to 0.038 for PHI. The PHI interval was narrower than under the reference 10 km spatial block design. Both diagnostic intervals retained the pattern observed with spatial grouping: the TNI interval remained entirely negative, while the PHI interval encompassed regional contrasts in both directions.

For the model relating PHI to TNI and region, the HGC coefficient of −0.041 had a spatial bootstrap interval from −0.113 to 0.027. Adding log route length, fitting a TNI-by-region interaction and restricting the analysis to the 90 routes within the common TNI range produced regional coefficient intervals that likewise extended across zero. Residual spatial association was greater in the Apuseni Mountains, where Moran's I was 0.440 with an exploratory permutation p-value of 0.0002, compared with 0.073 and 0.112 in the HGC region. This difference in residual structure accompanied the modest explanatory power of the conditional models.

Changing the PHI weights altered the balance between the opposing component contributions identified in **Fig. 8**. Across the 231 non-negative weight combinations, the HGC-minus-Apuseni median contrast ranged from −0.254 to 0.114. Positive contrasts occurred at 45.0% of the evaluated grid points and negative contrasts at 55.0%. These proportions describe the distribution of regional orderings across the specified weight grid.

Equal component weights produced a median contrast of −0.038, close to the reference value of −0.032. When the temperature component was omitted and the remaining weights were rescaled to sum to one, the contrast shifted to +0.104, with a spatial block-bootstrap interval from 0.003 to 0.173. Giving the assessment greater emphasis on solar potential and canopy openness therefore raised the HGC scores relative to the Apuseni Mountains.

The Dirichlet weight samples showed how individual routes changed position when ranked by decreasing PHI across all 103 itineraries. D72 appeared among the ten highest-scoring routes in 47.0% of the uniformly distributed weight samples and in 66.3% of the samples concentrated near the reference weights. The corresponding frequencies for D70 were 52.8% and 28.7%. D70 also showed a particularly broad range of positions under uniform weighting: its 5^{th} – 95^{th} percentile range of sampled ranks extended from 3 to 90, compared with 5 to 26 under weights concentrated near the reference scenario. Boga–Piatra Ciungilor–DJ 763 remained outside the ten highest-PHI routes in all samples under both weight distributions. These differences reflect the contrasting component profiles of the three itineraries and their response to changes in environmental emphasis.

All 24 processing combinations retained negative regional median contrasts for both indices **(Fig. 10)**. The TNI differences ranged from −0.083 to −0.046, and the PHI differences from −0.056 to −0.026. Variations in segment spacing, elevation smoothing, reference-mass allocation, percentile limits and horizon treatment changed the magnitude of the contrasts while preserving their direction.

Solar potential estimates were closely aligned between the horizons sampled along 16 and 32 azimuths. Across primary-route segments, the length-weighted mean absolute relative difference, using the 32-azimuth estimates as the reference, was 0.078% in the HGC region and 0.183% in the Apuseni Mountains. Including terrain-horizon shading reduced the length-weighted regional mean solar potential by 1.44% in the HGC region and 3.95% in the Apuseni Mountains relative to calculations using the astronomical horizon alone. Terrain screening therefore had a greater aggregate effect in the sampled Apuseni routes, while the two angular discretizations produced similar solar estimates within each region.

The regional comparisons also retained their direction when additional route categories were included. With the normalization calibrated on the primary sample held fixed, including the seven additional itineraries retained for route-selection sensitivity analysis increased the sample from 103 to 110 routes. The resulting HGC-minus-Apuseni median contrasts were −0.077 for TNI and −0.024 for PHI. Including the five fragments shorter than 500 m brought the sample to 115 routes and produced contrasts of −0.074 and −0.029, respectively. The expanded samples thus preserved the lower HGC medians for both indices, with a somewhat smaller PHI contrast than in the primary comparison.

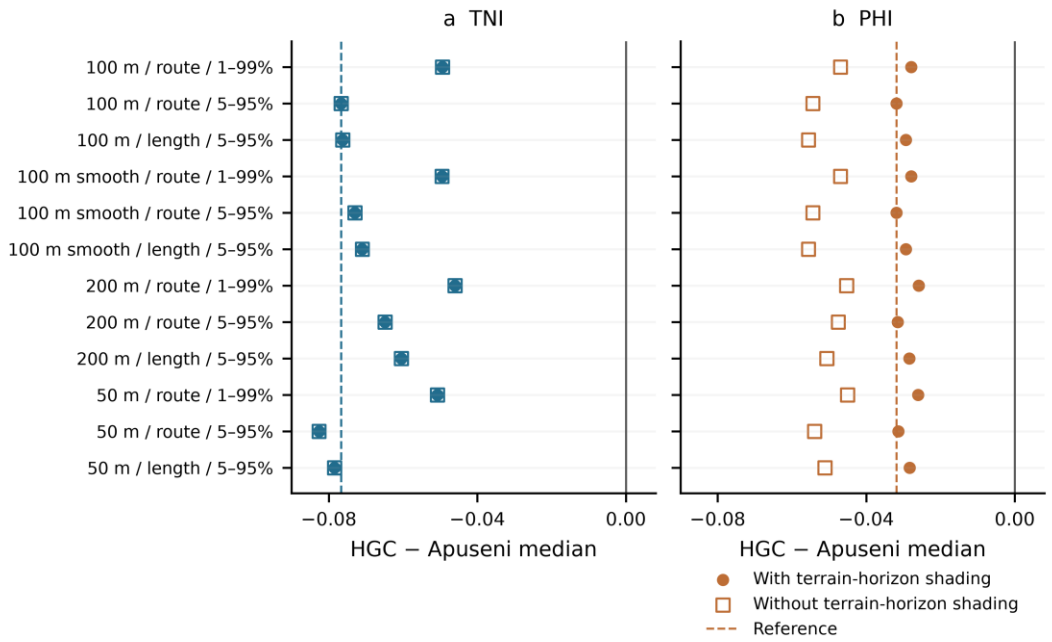


Fig. 10. Median HGC-minus-Apuseni contrasts across 24 processing variants. 'Route' and 'length' denote equal-region/equal-route and pooled length-weighted calibration; percentages denote normalization limits. Filled circles include terrain-horizon shading; open squares use the astronomical horizon alone. Dashed lines show the reference setting (100 m, route, 5–95%, terrain-horizon shading).

5. DISCUSSION

Terrain-related walking demand showed a more consistent regional contrast than summer environmental exposure. For PHI, the regional ordering depended on the balance between temperature, solar potential and canopy openness, and spatial resampling produced intervals encompassing contrasts in both directions. Route descriptions can preserve this distinction by presenting terrain demand and environmental exposure separately, alongside distance and estimated walking time. An itinerary may then be described as relatively undemanding in terms of slope while containing extended sections with little crown cover.

For D72, the practical addition to a visitor description is the location and duration of its long open section. A route map could identify where this section begins and where crown cover increases again, giving guides specific information to discuss when planning the walk with visitors. Such descriptions fit the links between walking tourism, local guiding and accommodation outlined by UNWTO (2019), and Romania's emphasis on rural tourism products and destination development (OECD, 2026). Their influence on route choice and visitor experience could subsequently be examined through responses to alternative descriptions, observed choices and reported thermal experience.

The purpose of the description also determines which components deserve attention. Crown-cover profiles and section duration are directly relevant to prolonged open walking, while temperature provides the broader climatic setting. This use of geographical information follows the activity-specific approach illustrated at Racoș by Lakatos et al. (2023), applied here to existing itineraries. In the Apuseni Mountains, the resulting route descriptions could accompany information about caves, scenery and opportunities for relaxation, reflecting the visitor interests examined by Telbisz et al. (2023).

Crown cover has a plausible ecological connection to summer walking conditions through the thermal buffering documented beneath forest canopies (De Frenne et al., 2019; Zellweger et al., 2020). The openness component represents this relationship through projected crown cover. Shade along an

actual path also varies with tree height, crown arrangement, the position of the path and solar geometry. Biometeorological approaches such as UTCI and RayMan examine thermal conditions through meteorological and radiation variables, with physiological interpretation linked to activity and personal characteristics (Bröde et al., 2012; Matzarakis et al., 2007). PHI serves the geographical comparison undertaken here, summarising background temperature, geometric solar potential and canopy openness within the stated assessment scenario.

The regional patterns describe the route alternatives supplied by the selected providers within the two processing footprints. Shared trail sections form part of that sample, and the spatial resampling and overlap-based checks examine how their grouping affects the comparisons. The environmental layers likewise represent different spatial supports. ERA5-Land contributes 37 unique grid cells along HGC routes and 19 along Apuseni routes, while the elevation and crown-cover layers resolve finer variation along the paths. Elevation-derived quantities follow the digital surface model, including vegetation and structures, and the solar estimates reflect the selected horizon distances and azimuths. The temperature and crown-cover components retain their respective reference periods of 1991–2020 and 2023.

Further work could add seasonal vegetation information from Sentinel-2 imagery to the crown-cover profiles, allowing descriptions to follow changes during the walking season (Drusch et al., 2012). The archived temperature series also offers a basis for examining longer-term climatic changes through trend estimation and uncertainty measures suited to serially correlated observations (Newey & West, 1987; Sen, 1968). These analyses would place the route profiles within their seasonal and historical environmental context.

6. CONCLUSIONS

The sampled HGC routes had lower slope-related walking demand than the Apuseni routes, with the regional TNI contrast retaining its direction across the tested processing and spatial grouping choices. Environmental exposure followed a more variable pattern. HGC routes had lower PHI under the reference weighting, although the spatial resampling interval included regional contrasts in both directions. Lower background temperature made the largest negative contribution to the difference in mean PHI, partly offset by greater solar potential and canopy openness. The tested processing variants preserved the regional ordering, while changes in component weights could reverse it.

At route level, the paired indices reveal combinations that are useful for walking-tourism information. D72's low terrain demand accompanies several kilometres of continuous open walking, while the shorter Boga–Piatra Ciungilor itinerary combines greater terrain demand with more crown cover. D70 illustrates the importance of duration when interpreting a high openness value. Presenting these characteristics alongside distance, ascent and modelled walking time gives visitors a more specific account of the walk they are considering.

Destination managers and guides could use the route profiles to identify long open sections, explain changes in walking conditions and distinguish itineraries offered within the same mountain destination. The component values are particularly useful where PHI rankings change with the assessment weights. Together, the indices and profiles provide a structured basis for route descriptions and for selecting sections that merit closer field assessment.

ACKNOWLEDGEMENT

The presented research was supported by the DOMUS scholarship program of the Hungarian Academy of Sciences.

REFERENCES

Bihor în imagini (n.d.) Hiking trails in Apuseni Natural Park. Route descriptions. Available at: https://www.bihorinimagini.ro/en/category/hiking-trails/hiking-trails-in-apuseni-natural-park/page/3/ (archived project source, 6 September 2026).

Bröde, P., Fiala, D., Błażejczyk, K., Holmér, I., Jendritzky, G., Kampmann, B., et al. (2012) Deriving the operational procedure for the Universal Thermal Climate Index (UTCI). *International Journal of Biometeorology*, 56(3), 481-494. https://doi.org/10.1007/s00484-011-0454-1

Buttke, D.E., Raynor, B. & Schuurman, G.W. (2023) Predicting climate-change induced heat-related illness risk in Grand Canyon National Park visitors. *PLOS ONE*, 18(8), e0288812. https://doi.org/10.1371/journal.pone.0288812

Copernicus Climate Change Service (C3S) (2019) ERA5-Land monthly averaged data from 1950 to present. Climate Data Store. Available at: https://doi.org/10.24381/cds.68d2bb30.

Copernicus Data Space Ecosystem (n.d.) Copernicus DEM. Product documentation. Available at: https://dataspace.copernicus.eu/explore-data/data-collections/copernicus-contributing-missions/collections-description/COP-DEM (accessed 2 October 2026).

Copernicus Land Monitoring Service (CLMS) (2024) Tree Cover Density 2018–Present, Europe, yearly, 10 m. Reference year used: 2023. Available at: https://doi.org/10.2909/e677441e-fb94-431c-b4f9-304f10e4dfd8.

De Frenne, P., Zellweger, F., Rodríguez-Sánchez, F., Scheffers, B.R., Hylander, K., Luoto, M., et al. (2019) Global buffering of temperatures under forest canopies. *Nature Ecology & Evolution*, 3(5), 744-749. https://doi.org/10.1038/s41559-019-0842-1

Dormann, C.F., McPherson, J.M., Araújo, M.B., Bivand, R., Bolliger, J., Carl, G., et al. (2007) Methods to account for spatial autocorrelation in the analysis of species distributional data: a review. *Ecography*, 30(5), 609-628. https://doi.org/10.1111/j.2007.0906-7590.05171.x

Drusch, M., Del Bello, U., Carlier, S., Colin, O., Fernandez, V., Gascon, F., et al. (2012) Sentinel-2: ESA's Optical High-Resolution Mission for GMES Operational Services. *Remote Sensing of Environment*, 120, 25-36. https://doi.org/10.1016/j.rse.2011.11.026

Dubayah, R. & Rich, P.M. (1995) Topographic solar radiation models for GIS. *International journal of geographical information systems*, 9(4), 405-419. https://doi.org/10.1080/02693799508902046

Ďuračiová, R. & Pružinec, F. (2022) Effects of Terrain Parameters and Spatial Resolution of a Digital Elevation Model on the Calculation of Potential Solar Radiation in the Mountain Environment: A Case Study of the Tatra Mountains. *ISPRS International Journal of Geo-Information*, 11(7), 389. https://doi.org/10.3390/ijgi11070389

Fu, P. & Rich, P.M. (2002) A geometric solar radiation model with applications in agriculture and forestry. *Computers and Electronics in Agriculture*, 37(1-3), 25-35. https://doi.org/10.1016/S0168-1699(02)00115-1

Fung, T. & Wong, F.K.K. (2007) Ecotourism planning using multiple criteria evaluation with GIS. *Geocarto International*, 22(2), 87-105. https://doi.org/10.1080/10106040701207332

Greco, S., Ishizaka, A., Tasiou, M. & Torrisi, G. (2019) On the Methodological Framework of Composite Indices: A Review of the Issues of Weighting, Aggregation, and Robustness. *Social Indicators Research*, 141(1), 61-94. https://doi.org/10.1007/s11205-017-1832-9

Higgins, C.D. (2021) Hiking with Tobler: Tracking Movement and Calibrating a Cost Function for Personalized 3D Accessibility. *Findings*. https://doi.org/10.32866/001c.28107

HRTracks (n.d.) Harghita County hiking routes: route names and GPX downloads (in Hungarian and Romanian). Available at: https://hrtracks.gisit.ro/indexhu.html (archived project source, 6 September 2026).

Irmischer, I.J. & Clarke, K.C. (2018) Measuring and modeling the speed of human navigation. *Cartography and Geographic Information Science*, 45(2), 177-186. https://doi.org/10.1080/15230406.2017.1292150

Lahdelma, R., Hokkanen, J. & Salminen, P. (1998) SMAA - Stochastic multiobjective acceptability analysis. *European Journal of Operational Research*, 106(1), 137-143. https://doi.org/10.1016/S0377-2217(97)00163-X

Lahiri, S.N. (2003) Resampling Methods for Dependent Data. New York: Springer. https://doi.org/10.1007/978-1-4757-3803-2

Lakatos, J., Magyari-Sáska, Z. & Dombay, S. (2023) A GIS-based analysis for ecotourism suitability in a geological complex area of Carpathians. *Geographia Technica*, 18(1), 149-160. https://doi.org/10.21163/GT_2023.181.11

Malczewski, J. (2006) GIS-based multicriteria decision analysis: a survey of the literature. *International Journal of Geographical Information Science*, 20(7), 703-726. https://doi.org/10.1080/13658810600661508

Matzarakis, A., Rutz, F. & Mayer, H. (2007) Modelling radiation fluxes in simple and complex environments—application of the RayMan model. *International Journal of Biometeorology*, 51(4), 323-334. https://doi.org/10.1007/s00484-006-0061-8

Moran, P.A.P. (1950) NOTES ON CONTINUOUS STOCHASTIC PHENOMENA. *Biometrika*, 37(1-2), 17-23. https://doi.org/10.1093/biomet/37.1-2.17

Muñoz-Sabater, J., Dutra, E., Agustí-Panareda, A., Albergel, C., Arduini, G., Balsamo, G., et al. (2021) ERA5-Land: a state-of-the-art global reanalysis dataset for land applications. *Earth System Science Data*, 13(9), 4349-4383. https://doi.org/10.5194/essd-13-4349-2021

Newey, W.K. & West, K.D. (1987) A Simple, Positive Semi-Definite, Heteroskedasticity and Autocorrelation Consistent Covariance Matrix. *Econometrica*, 55(3), 703–708. https://doi.org/10.2307/1913610

OECD (2026) OECD Tourism Trends and Policies 2026. Paris: OECD Publishing. Romania country profile. https://doi.org/10.1787/3fd3cd75-en

OECD, European Union and European Commission Joint Research Centre (2008) Handbook on Constructing Composite Indicators: Methodology and User Guide. Paris: OECD Publishing. https://doi.org/10.1787/9789264043466-en

Roberts, D.R., Bahn, V., Ciuti, S., Boyce, M.S., Elith, J., Guillera-Arroita, G., et al. (2017) Cross-validation strategies for data with temporal, spatial, hierarchical, or phylogenetic structure. *Ecography*, 40(8), 913-929. https://doi.org/10.1111/ecog.02881

Saisana, M., Saltelli, A. & Tarantola, S. (2005) Uncertainty and Sensitivity Analysis Techniques as Tools for the Quality Assessment of Composite Indicators. *Journal of the Royal Statistical Society Series A: Statistics in Society*, 168(2), 307-323. https://doi.org/10.1111/j.1467-985X.2005.00350.x

Salvamont Bihor (n.d.) Hiking routes in Pădurea Craiului (in Romanian). Available at: https://www.salvamontbihor.ro/page/trasee-turistice-padurea-craiului (archived project source, 6 September 2026).

Scott, D., Hall, C.M. & Gössling, S. (2019) Global tourism vulnerability to climate change. *Annals of Tourism Research*, 77, 49-61. https://doi.org/10.1016/j.annals.2019.05.007

Sen, P.K. (1968) Estimates of the Regression Coefficient Based on Kendall's Tau. *Journal of the American Statistical Association*, 63(324), 1379-1389. https://doi.org/10.1080/01621459.1968.10480934

Steegen, S., Tuerlinckx, F., Gelman, A. & Vanpaemel, W. (2016) Increasing Transparency Through a Multiverse Analysis. *Perspectives on Psychological Science*, 11(5), 702-712. https://doi.org/10.1177/1745691616658637

Szakács, A. & Kovacs, M. (2022) Volcanic Landforms and Landscapes of the East Carpathians (Romania) and Their Geoheritage Values. *Land*, 11(7), 1064. https://doi.org/10.3390/land11071064

Telbisz, T., Imecs, Z., Máthé, A. & Mari, L. (2023) Empirical Investigation of the Motivation and Perception of Tourists Visiting the Apuseni Nature Park (Romania) and the Relationship of Tourism and Natural Resources. *Sustainability*, 15(5), 4181. https://doi.org/10.3390/su15054181

Tobler, W. (1993) Three presentations on geographical analysis and modeling. NCGIA Technical Report 93-1. Santa Barbara: University of California. Available at: https://escholarship.org/uc/item/05r820mz (accessed 2 October 2026).

Visit Harghita (n.d.) Vârghiș Gorge. Geographic description. Available at: https://www.visitharghita.com/en/places/varghis-gorge (accessed 2 October 2026).

World Tourism Organization (UNWTO) (2019) Walking Tourism – Promoting Regional Development. Madrid: UNWTO. https://doi.org/10.18111/9789284420346

Zellweger, F., De Frenne, P., Lenoir, J., Vangansbeke, P., Verheyen, K., Bernhardt-Römermann, M., et al. (2020) Forest microclimate dynamics drive plant responses to warming. *Science*, 368(6492), 772-775. https://doi.org/10.1126/science.aba6880